Aberrant Population Receptive Fields in Human Albinism

Ethan J. Duwell[a], Erica N. Woertz[b], Jedidiah Mathis[c], Joseph Carroll[a,b,d], Edgar A. DeYoe[c]*

[a]Department of Biophysics, Medical College of Wisconsin, 8701 Watertown Plank Road, Milwaukee, WI 53226, USA

[b]Department of Cell Biology, Neurobiology, & Anatomy, Medical College of Wisconsin, 8701 Watertown Plank Road, Milwaukee, WI 53226, USA

[c]Department of Radiology, Medical College of Wisconsin, 8701 Watertown Plank Road, Milwaukee, WI 53226, USA

[d]Department of Ophthalmology & Visual Sciences, Medical College of Wisconsin, 925 N. 87th Street, Milwaukee, WI 53226, USA

*Corresponding Author: Edgar DeYoe, Department of Radiology, Medical College of Wisconsin, 8701 Watertown Plank Road, Milwaukee, WI 53226; deyoe@mcw.edu

Manuscript: Pages - 42; Tables - 1; Figures - 6; Color Figures - 6; Supplemental Figures - 0

Acknowledgments: The authors would like to thank Melissa Wilk and Erin Curran for their contributions to this work. We would also like to thank Murray Brilliant for his contributions to our genetic testing. Research reported in this publication was supported by the National Eye Institute, the National Institute of General Medical Sciences, and the National Center for Advancing Translational Sciences of the National Institutes of Health under award numbers TL1TR001437, T32GM080202, T32EY014537, P30EY001931, and R01EY024969. This investigation was conducted in a facility constructed with support from Research Facilities

Improvement Program, Grant Number C06RR016511, from the National Center for Research Resources, National Institutes of Health. The content is solely the responsibility of the authors and does not necessarily represent the official views of the National Institutes of Health. This work was also supported by Vision for Tomorrow.

Conflicts of Interest: The authors declare no competing financial interests.

Abstract:

Retinotopic organization is a fundamental organizational feature of visual cortex thought to play a vital role in encoding spatial location. One important aspect of normal retinotopic organization is the contralateral representation of the right and left hemifields in visual cortex. In human albinism, the temporal retinal afferents decussate pathologically at the optic chiasm resulting in partially superimposed right and left hemifield representations in each hemisphere of visual cortex. Thus, albinism provides a natural model of aberrant retinotopy in which to study the development and function of retinotopic maps. Previous fMRI studies in human albinism suggest that the right and left hemifields are superimposed in a mirror-symmetric manner such that each imaging voxel responds to two regions in visual space mirrored across the vertical meridian. However, to date no group has explicitly attempted to model the receptive field properties of single voxels in albinism. Here we used traditional fMRI retinotopic mapping techniques in conjunction with population receptive field (pRF) modeling in subjects with albinism to fit each voxel's rotating wedge timecourse in V1-V3 with both single and dual pRF models. We find that most subjects with albinism (but not controls) have sizable clusters of voxels with convincing dual pRFs often corresponding to regions of R-L hemifield overlap. However, not all dual pRFs were mirror symmetrical across the vertical meridian. These asymmetric dual pRFs are not predicted by currently accepted models and suggest that retinocortical miswiring in albinism may be more complicated and heterogenous than previously appreciated.

Significance Statement:

In albinism, the temporal retinal afferents decussate aberrantly at the optic chiasm during development causing partially superimposed right and left hemifield maps in visual cortex. The currently accepted model of retinocortical miswiring in human albinism suggests that these maps are superimposed in a mirror-image fashion such that single locations in visual cortex should respond to two symmetric locations in opposite visual hemifields. To test this, we modeled population receptive fields of individual voxels as single or dual Gaussian sensitivity profiles, fitting the predicted responses to fMRI retinotopic mapping data. For the first time, our results reveal dual pRFs in cortical visual areas V1-V3 in subjects with albinism. However, some subjects had highly asymmetric dual pRFs, indicating that retinocortical miswiring in albinism is more heterogenous and complex than suggested by the "mirror symmetric" model.

Introduction

Retinotopic organization is one of the most fundamental and widely-described organizational principles of visual cortex. Present at every level of the visual hierarchy, the retinotopic organization of visual cortex is thought to play a vital role in the brain's ability to encode visual-spatial location. The establishment of such retinotopic organization requires a surprising degree of specificity during development; however, the mechanisms which govern the emergence of retinotopically organized visual-cortical maps are still not fully known. One historically promising route toward understanding the development and function of retinotopic maps is to study pathological cases in which normal retinotopy is disrupted.

Albinism is a well-known genetic syndrome characterized by disrupted melanin synthesis causing hypopigmentation of the eyes, and often the skin and hair. However, albinism is also associated with aberrant decussation of the temporal retinal afferents at the optic chiasm such that each cortical hemisphere receives substantial input from both the right and left visual hemifields of the same eye (Morland et al., 2001; Hoffmann et al., 2003; Kaule et al., 2014). This results in superimposed retinotopic maps of significant portions of <u>opposite</u> hemifields within each hemisphere of occipital visual cortex. In healthy, control subjects, each hemisphere contains superimposed maps of the <u>same</u> contralateral hemifield from each eye (Horton and Hoyt, 1991). Thus, the pattern of miswiring in albinism represents a major disruption of normal retinotopic organization.

Previous fMRI mapping studies in albinism suggest that the right and left hemifield representations are superimposed in a precise manner such that each voxel responds to two regions at roughly mirror image locations across the vertical meridian (Hoffmann et al., 2003). This pattern is generally consistent with the "true albino" pattern of hemifield superposition previously described in albino primates in which ocular dominance columns are supplanted by hemifield dominance columns (Guillery et al., 1984; Hoffmann and Dumoulin, 2015). This

columnar pattern was recently confirmed in high-resolution fMRI studies in human achiasma but has yet to be confirmed in albinism (Olman et al., 2018). More recently, investigators have used single voxel population receptive field (pRF) modeling techniques to demonstrate the existence of single voxels with mirror symmetric bilateral (dual) pRFs in achiasma and FHONDA syndrome (Hoffmann et al., 2012; Ahmadi et al., 2018). These studies have assumed that subjects with albinism should present with the same mirror symmetric, dual pRF topographies. However, this may not be the case as the genetic determinants and nature of retinocortical miswiring differ in achiasma, FHONDA, and albinism (Hoffmann and Dumoulin, 2015; Ahmadi et al., 2018). Moreover, albinism itself is a heterogeneous syndrome with a wide variety of genetic and phenotypic subtypes (Oetting et al., 1994; Simeonov et al., 2013; Montoliu et al., 2014; Wilk et al., 2014b; Prieur and Rebsam, 2017). In a previous study (Woertz et al., 2019), we describe significant variation in the pattern of hemifield eccentricity representations in subjects with albinism with retinotopy that ranges from nearly normal to highly aberrant, thus suggesting that pRF properties in albinism might also vary considerably.

In this study, we used traditional fMRI retinotopic mapping in combination with population receptive field modeling of voxels in V1-V3 of subjects with genetically-confirmed albinism. We tested the hypothesis that cortical retinotopic organization in albinism is aberrant and that this is associated with voxels in visual cortex having bilateral (dual) pRFs. Our results show that dual pRFs are indeed present in subjects with albinism but that they are uniquely asymmetric in some individuals. They also are not uniformly distributed within zones of opposed hemifield overlap, but rather are grouped into localized clusters. Such unexpected variation suggests that retinocortical miswiring in albinism is more variable and complex than suggested by a simple model of aberrant left-right decussation at the optic chiasm.

Materials and Methods

Subjects

Six subjects with albinism (4 females, 2 males; aged 15-31 years) with minimal nystagmus and five subjects with no prior ocular or cortical pathology (2 females, 3 males; aged 20-25 years) were recruited for this experiment. One subject with albinism was excluded from further analysis due to significant motion artifacts in the fMRI data (male, age 15 years), one control subject was excluded due to poor alertness during fMRI. Genetic information and demographics for each albinism subject are listed in **Table 1** below. Retinal features as well as cortical magnification in these subjects are described in detail elsewhere (Wilk et al., 2014a; Wilk et al., 2017; Woertz et al., 2019). It is also notable that subjects 2 and 4 are siblings with identical mutations. The study was in accordance with the Declaration of Helsinki and approved by the Institutional Review Board of the Medical College of Wisconsin. All subjects provided written informed consent after explanation of the nature and possible risks and benefits of the study.

Table 1: Genetics and Demographics for Subjects with Albinism

Subject	ID**	Age (y)	Sex	BCVA	Phenotype^	Mutations
1	JC_10227	19	F	20/40 (OU)	OCA2	*OCA2* c.1327G>A; p.V443I *TYR* c. 575C>A; p.S192Y
2*	JC_0492	31	F	20/25 (OU)	OCA1B	*TYR* c.1147G>A; p.D383N *TYR* c.1217C>T; p.P406L
3	JC_10230	18	F	20/50 -2 (OU)	OCA1B	*TYR* c. 575C>A; p.S192Y *TYR* c. 575C>A; p.S192Y *TYR* c. 1205G>A; p.R402Q *TYR* c. 1265G>A; p.R422Q
4*	JC_0493	23	F	20/20- (OU)	OCA1B	*TYR* c.1147G>A; p.D383N *TYR* c.1217C>T; p.P406L
5	JC_10093	19	M	20/100 +2 (OD)	OA	*GPR143* c.346T>G; p.C116G

				20/80 +2 (OS)		*TYR* c. 1205G>A; p.R402Q *TYR* c. 1205G>A; p.R402Q
6***	JC_10278	19	M	20/32 (OU)	OCA1B	*TYR* c.286_287insA; fs *TYR* c. 575C>A; p.S192Y *TYR* c. 575C>A; p.S192Y

*Subjects are sisters

**ID used in Wilk *et al.* (2014) & Wilk *et al.* (2017)

*** Excluded due to motion artifact

^OCA=oculocutaneous albinism; OA=ocular albinism (X-linked)

fMRI Visual Stimuli

All visual stimuli for fMRI were presented on a back-projection screen mounted on the MRI head coil. A BrainLogics BLMRDP-A05 MR digital projector (Puckett and DeYoe, 2015) was used with a ViSaGe MKII visual stimulus generator (Cambridge Research Instruments) in conjunction with custom MATLAB software. Stimuli subtending a maximum of 20° eccentricity included conventional expanding ring and rotating wedge retinotopic mapping stimuli (DeYoe et al., 1996). Rings and wedges were composed of black and white counterphase flickering (8 Hz) circular checkerboards with check size and ring width scaled with eccentricity. Stimuli were presented on a uniform gray background. All subjects were instructed to continually fixate a marker at the center of the screen. To enhance stable fixation, thin, black radial lines extending from fixation to the edge of the display were present continuously in all tasks.

To avoid collecting largely redundant MRI data, for our control subjects the retinotopic mapping data were obtained using slightly different experimental protocols for the controls and subjects with albinism. Due to the temporal phase mapping methods used in this study, retinotopic parameters (eccentricity, polar angle) that are encoded by the timing of the fMRI responses did not appear to be significantly affected by the stimulus differences. For subjects with albinism, the wedge stimuli subtended 45° polar angle, and for control subjects the wedges subtended 90°. All subjects viewed both ring and wedge stimuli binocularly with full-

field stimulation. Additionally, for subjects with albinism the expanding ring stimuli were presented to the right and left hemifields in separate runs and were tested separately for each eye. The hemifield ring stimuli were identical to the full field version, except that one hemifield was masked to match the grey background. For control subjects, the ring stimulus expanded from the center to the periphery in 40 s. and was repeated five times per run. For subjects with albinism, both the full-field and hemifield ring stimuli expanded from 0.8° eccentricity to the periphery in 60 s. and were repeated five times per run. For subjects with albinism, the center of the display consisted of a circular black and white disc (similar to a radioactivity symbol) with a radius of 0.8° that flickered at random intervals not synchronized to the rings or wedges presentation. To control attention, subjects were instructed to press and hold a button whenever the central disc flickered.

fMRI Stimulus Paradigm

Control subjects completed all imaging during a single session. Subjects with albinism completed imaging during two sessions: the right eye hemifield expanding ring tasks in the first session, and all remaining tasks in the second session. All monocular hemifield runs were repeated five times and binocular full-field runs were repeated three times. For monocular stimuli, repetitions of the right and left hemifield stimuli were interleaved; for full-field stimuli, repetitions of the expanding ring and rotating wedge were interleaved. After each fMRI run, the subject was asked to rate their alertness on a scale from 1-5 (1 being asleep and 5 being fully awake). This measure was intended to control for subjects' alertness which can affect the quality of data and potentially can be used as an exclusion criterion. One control subject was excluded due to poor alertness.

fMRI Acquisition

Scans were completed using a 3.0 Tesla General Electric Signa Excite 750 MRI system at the Medical College of Wisconsin. A custom 32-channel RF/Gradient head coil and a T2*-weighted gradient-echo EPI pulse sequence (TE = 25 ms, TR = 2 s, FA = 77°) were used. The 96 x 96 acquisition matrix (Fourier interpolated to 128 x 128) had frequency encoding in the right-left axial plane, phase encoding in anterior-posterior direction and slice selection in the axial direction. The FOV was 240 mm and included 29 axial slices covering the occipital lobe and adjacent portions of the temporal and parietal lobes with a slice thickness of 2.5 mm, yielding a raw voxel size of 1.875 x 1.875 x 2.5 mm. For anatomical scans, a T1-weighted, spoiled gradient recalled echo-planar at steady state (SPGR) pulse sequence was used (TE = 3.2 ms, TR = 8.2 ms, FA = 12°) with a 256 x 224 acquisition matrix (Fourier interpolated 256 x 256). The FOV was 240 mm, and 180 slices with a slice thickness of 1.0 mm, yielding raw voxel sizes of 0.938 × 0.938 × 1.0 mm^3. The SPGR scans were subsequently resampled to 1.0 mm^3. A sync pulse from the scanner at the beginning of each run triggered the onset of visual stimuli.

Analysis Software

All fMRI data were analyzed using the AFNI/SUMA package (version: AFNI_18.0.22) (Cox, 1996). Surface models were produced from the high resolution SPGR images using Freesurfer (version 5.1.0 and 5.3.0, http://surfer.nmr.mgh.harvard.edu/) with the 'recon-all' function. Single voxel time-course modeling was performed using custom software in MATLAB (R2017b).

fMRI pre-processing

fMRI pre-processing was performed in the following order: reconstruction, volume registration, averaging of the time courses, removal of the initial magnetization transients,

alignment. Volumes from all individual runs in an interleaved block were registered to the middle volume of the first run in the block using AFNI 3dVolreg. Individual runs for each functional task were averaged using AFNI 3dMean to produce average time courses. The before and after periods were removed using AFNI 3dcalc.

For subjects with albinism, we attempted to minimize bias in the alignment of functional scans from either of the two sessions to the reference anatomy by using a modified version of the align_across_days.csh script available on the AFNI and NIfTI server (https://afni.nimh.nih.gov/sscc/staff/glend/align_html/alignacross2sessions.html). In this script, the reference SPGR anatomical images from both sessions were skull-stripped using AFNI 3dSkullStrip, aligned using AFNI align_epi_anat.py script, and averaged using AFNI 3dMean to create an average reference anatomy for the two sessions. All individual and average functional runs were then aligned to these average reference anatomies using the align_epi_anat.py script. For control subjects, all data were acquired in a single session, so the creation of an average reference anatomy was not necessary. The alignment of functional runs for control subjects was otherwise identical to subjects with albinism.

Phase Encoded Retinotopic Maps

The spatial distributions of significant fMRI responses for each functional task were displayed as phase encoded retinotopic activation maps. Significant responses were identified by cross correlating the empirical time course data for each voxel with a reference waveform using AFNI 3ddelay (Bandettini et al., 1993; Saad et al., 2003; Datta and DeYoe, 2009). This analysis produces the correlation coefficient and phase values at the phase offset of maximum correlation for each voxel. The reference waveform used for this phase mapping procedure was a binary square wave describing the stimulus cycles convolved temporally with the “Cox Wide” estimation of the hemodynamic response function (HRF). The 3ddelay analysis was

performed on both unsmoothed data and on data that were spatially smoothed with a 3.75 mm spherical kernel using AFNI 3dLocalstat. The smoothed full field retinotopy data were only used for the purposes of visual area ROI mapping.

Visual Area Mapping

The correlation analysis described above was performed on the smoothed full field phase encoded retinotopy data, and the results were projected onto cortical surface models in AFNI/SUMA. These phase encoded polar angle and eccentricity maps were used to identify and map visual areas V1-V3 in both albinism subjects and controls using criteria previously reported by a number of labs (Sereno et al., 1995; DeYoe et al., 1996; Engel et al., 1997; Sereno et al., 2001; Pitzalis et al., 2006; Hansen et al., 2007; Swisher et al., 2007; Wandell et al., 2007; Amano et al., 2009; Arcaro et al., 2009; Silver and Kastner, 2009; Pitzalis et al., 2010; Wandell and Winawer, 2011). Visual area ROIs drawn on the cortical surface models were then transformed back to the volumetric domain using AFNI's 3dSurf2Vol.

Identifying Cortical Zones of Right-Left Hemifield Overlap in Albinism

To identify cortical regions responding to both the right and left hemifields in each subject with albinism, the monocular right and left hemifield eccentricity maps from both eyes were thresholded to a minimum correlation coefficient of 0.35, binarized, and then logically combined using AFNI's 3dcalc to generate hemifield overlap maps. Any voxel which responded above threshold in both a left and right hemifield stimulation condition was included in that subject's hemifield overlap ROI. Voxels which responded to only a single hemifield were included in that subject's non-overlap ROI.

Population Receptive Field Modeling

Both single and dual Gaussian population receptive field (pRF) models were optimized for each responsive voxel to fit the rotating wedge time-course data in visual areas V1-V3 for subjects with albinsim and controls. The procedure was inspired by methods developed by Dumoulin et al. (Dumoulin and Wandell, 2008) but was implemented independently using custom Matlab software (Puckett and DeYoe, 2015). The modeling algorithm uses properties of the stimuli, tasks, and BOLD hemodynamics in conjunction with estimates of the pRF to generate a predicted fMRI waveform. This predicted waveform was then fit to the empirical time-course data yielding an error signal which was used to drive an iterative optimization of the Gaussian model parameters so as to fit the empirical data most accurately. Single pRFs were modeled as a simple 2D Gaussian:

$$(1)\ g(x,y) = Ae^{-\frac{(x-x_0)^2+(y-y_0)^2}{2\sigma_1^2}}$$

where (x_0, y_0) is the center position, σ is the standard deviation of the distribution, and A is an amplitude scaling factor. Dual pRFs were modeled as the sum of two independent 2D Gaussians:

$$(2)\ g(a,b,x,y) = A_1e^{-\frac{(a-a_0)^2+(b-b_0)^2}{2\sigma_1^2}} + A_2e^{-\frac{(x-x_0)^2+(y-y_0)^2}{2\sigma_2^2}}$$

where (a_0,b_0) and (x_0,y_0) are the centers of the two Gaussians, σ_1 and σ_2 are the standard deviations of the two Gaussians, and A_1 and A_2 are the amplitude scaling factors.

The modeling procedure began by multiplying an initial pRF estimate with the spatial pattern of the stimulus and integrating over space at each timepoint to generate an ideal 'neural' response waveform. This ideal response was then convolved temporally with an estimate of the HRF to produce a predicted fMRI response. The residual sum squared error (RSS) between this predicted response and the empirical fMRI waveform was then computed.

The RSS error signal then drove an iterative optimization of the location, standard deviation, and amplitude parameters of the model searching for the combination which produced the minimum error. Optimization began with a coarse search of all possible (a_0,b_0) and (x_0,y_0) starting positions limited to the voxel's preferred eccentricity as determined by the full field expanding ring experiment. Using the starting positions established by the coarse search, polar angle, σ, and A were refined in a two-pass, coarse-to-fine fashion using an unconstrained nonlinear optimization algorithm (Matlab's fminsearch algorithm) to obtain an optimal fit to the empirical rotating wedge fMRI waveform.

This process was performed twice for each voxel: once with the single Gaussian pRF model, and again with the dual Gaussian model. We emphasize that for the dual Gaussian model, each Gaussian was optimized independently. Previous papers performing dual receptive field modeling in achiasma and other disorders have restricted the two receptive fields to be at mirror image locations either across the vertical meridian, horizontal meridian, or fixation (Hoffmann et al., 2012; Ahmadi et al., 2018). By allowing the two Gaussians to be optimized independently, our model tests the possibility that dual pRFs in albinism may be arranged at any combination of angular positions at a given eccentricity.

Voxel Selection

All of our quantitative analyses were performed only on voxels falling within our V1-V3 visual area ROIs. Selection criteria varied slightly in each separate analysis. To be included in our hemifield overlap analysis, voxel responses were required to achieve a correlation coefficient greater than 0.35 on at least 1 of the 4 hemifield stimulation conditions. For voxels to be included in our pRF analysis, one of the two pRF models must have explained a minimum of 25% of the total timecourse variance for that voxel. The percent variance explained by each model was calculated using **Equation 3** below. For inclusion in our analysis of the incidence of

dual pRF voxels in hemifield overlap vs. non overlap zones in albinism, voxels were required to meet both of the criteria above.

Model Comparison

The single and dual pRF model fits for each voxel were compared based on the difference in timecourse variance explained by the two respective models. The percent variance explained (%VE) by each respective model was computed on a voxel-wise basis using the following equation:

$$(3)\ \ \%VE = 100 \times \left(\frac{TSS-RSS}{TSS}\right)$$

Where TSS is the total sum of squares for the voxel timecourse and RSS is the residual sum of squared error from the model fitting. The difference in variance explained (ΔVE) by the dual and single pRF models was then computed for each voxel in the following manner:

$$(4)\ \Delta VE = \%VE_{dual} - \%VE_{single}$$

Where $\%VE_{dual}$ and $\%VE_{dual}$ are the percent variance explained by the dual and single pRF models respectively. Any given voxel was considered to have dual pRFs if that voxel was part of a contiguous (faces touching) cluster of 10+ voxels in which ΔVE was greater than or equal to 8% for each voxel in the cluster. Voxels not meeting this criterion were considered single pRF voxels. However, to be consistent, single pRF voxels were also required to belong to a cluster of 10+ single pRF voxels. Clustering was done using AFNI's 3dClusterize.

Dual pRF Symmetry

For all dual pRF voxels in albinism, the degree to which the dual pRFs were symmetric across the vertical meridian was assessed by computing the angle θ between the two pRF centers with respect to the horizontal meridian:

$$(5)\ \theta = Tan^{-1}\left(\frac{y_2 - y_1}{x_2 - x_1}\right)$$

Where (x1, y1) are the Cartesian coordinates for pRF center 1 and (x2, y2) are the coordinates for pRF center 2. The absolute values of these angles can range from 0°-90°. Since the dual pRF components were constrained to be at the same eccentricity, an angle of 0° indicated symmetry across the vertical meridian, and 90° indicated symmetry across the horizontal meridian. Histograms of dual pRF angle θ were generated for each albinism subject. Brain maps were also generated for each subject to plot the distribution of dual pRF angle θ across the cortical surface.

Results

Aberrant Retinotopic Organization in Albinism

As reported in the previous literature (Morland et al., 2001; Hoffmann et al., 2003; Kaule et al., 2014; Prieur and Rebsam, 2017), we observed overlapping representations of both left and right hemifields within each cerebral hemisphere of all our subjects with albinism. **Fig 1A**,**B** displays inflated cortical surface maps of the left hemisphere of one representative subject (subject 5). In this case, hemifield expanding ring stimuli were presented monocularly to the right eye. The eccentricity color code is shown in the upper left of **Fig 1A,B**. By visual inspection, the right and left hemifield eccentricity maps appear to be grossly in register but the aberrant left hemifield representation (B) was less complete than the normal right hemifield representation (A) so that the two maps only partially overlap. The foveal representation in this subject, which should be at the occipital pole, was reduced relative to our control subjects, as previously described in (Woertz et al., 2019).

The right and left hemifield representations in **Fig 1A**,**B** are combined logically in **Fig 1C** to form a right-left hemifield overlap map. In this map the blue regions responded exclusively to the right hemifield, yellow regions responded exclusively to the left hemifield, and the green 'overlap' regions responded to both hemifields. As displayed in **Fig 1C**, irregular bands of hemifield overlap (green) alternate with right hemifield monocular bands (blue) repeated both ventrally and dorsally in V1, V2 and V3 (black outlines). It is notable that the hemifield overlap zones (green) seemed to be roughly centered on representations of the vertical meridia that mark the V1-V2 boundaries while tending to avoid horizontal meridian representations that typically are associated with the middle of V1 and the V2/V3 borders (blue in **Fig 1C**).

The extent of hemifield overlap is quantified in **Fig 1D** for occipital visual areas V1-V3 for each of our five subjects with albinism. Here, data were combined across all stimulus eye conditions and hemispheres. To be classified as "overlapping", a voxel was required to

respond above threshold to both a right and left hemifield stimulus regardless of the eye stimulated. Within individual subjects, the percent overlap tended to be similar across V1-V3. However, there were considerable differences in the mean overlap across subjects with values ranging from 30%-50%.

pRFs in Albinism

The partial overlap of opposite hemifield representations in visual cortex gives rise to a complex mix of voxels with either single or dual responses to the rotating wedge stimulus. As illustrated in **Fig 2A** (left), the unusual dual responses (green traces) were easily identified in the rotating wedge timecourse data since they responded with ten robust peaks even though the wedge rotation had only five cycles. Yet within the same individual, other voxels responded to the same stimulus with the more typical 5 peaks (**Fig 2A** right). These results are consistent with some voxels responding to two visual field loci per cycle while other voxels respond to a single locus per cycle. To test this quantitatively, we fit each voxel's timecourse with both a single Gaussian and a dual Gaussian pRF model. In the top row of **Fig 2A,** we display the timecourse predicted by the single pRF model (black trace) and in the bottom row we display the dual pRF prediction. For the voxel illustrated in the left panel of **Fig 2A**, the dual Gaussian pRF model is able to fit all ten response peaks whereas the single Gaussian model only fits half the peaks. As a result there is a substantial difference in variance explained by the two models (75.7% vs. 47.2%). However, in the right voxel timecourse there are only 5 peaks to fit. Consequently, the additional Gaussian parameters of the dual model provide less benefit, and there is little difference in variance explained by the two models (73.4% vs. 75.5%). (Note: Since the two pRF components are fit independently, they tend to be forced into the same visual field locations when the empirical waveform has only 5 peaks, thus the 2 models tend to explain the same amount of variance.)

Fig 2B shows the voxel-wise difference in variance explained (ΔVE = %VE Dual - %VE Single) by the two models as a colored pattern across the cortical surface for albinism subject 5. There are clearly large clusters of voxels (yellow patch) in which the dual pRF model explains substantially more variance than the single pRF model, sometimes as much as an additional 40% of the total timecourse variance for the voxel.

Fig 2C displays the results of a single versus dual pRF clustering analysis (see Methods) for the same subject. In this analysis, a "dual pRF voxel" must be part of a cluster of 10+ voxels in which ΔVE is greater than 8% for all voxels in the cluster. Voxels not meeting this criterion are considered 'single pRF voxels' but also must meet a clustering threshold of 10. As displayed in **Fig 2D**, the dual pRF model explains significantly more timecourse variance (17%) than the single pRF model in the clusters deemed to be 'dual pRF clusters' (two tailed t test, $p < 0.001$) The difference in variance explained by the two models in the single pRF clusters was also statistically significant, but of much smaller magnitude (1%). This relationship for the albinism group was also evident in each individual subject.

Incidence of Dual pRF Voxels in V1-V3 in Albinism Relative to Controls

Voxels meeting our dual pRF criteria were observed in V1, V2, and V3. **Fig 3A** displays examples of dual pRF voxels' rotating wedge timecourses in V1-V3 in a representative subject with albinism. Again, the green traces are the empirical rotating wedge timecourses, and the black traces are the modeled timecourses. The corresponding dual pRF models represented in visual space are shown in the right column. Note that these voxels all responded to bilateral locations in opposite hemifields. The mean incidence of dual pRF voxels for both albinism and control groups is summarized in **Fig 3B** for V1, V2, and V3 separately as well as combined. Albinism subjects had significantly higher incidence of dual pRF voxels than controls in every visual area (heteroscedastic two tailed t tests for V1, V2, and V3, respectively: $p = 0.02$, $p <$

0.001, p = 0.03) as well as combined across visual areas (p = 0.01). Dual pRFs in subjects with albinism comprised over 10% of responding voxels in V1 to less than 4% in V2. In contrast, the overall incidence of dual pRFs in control subjects was less than 1%.

Dual pRF Distribution Relative to Hemifield Overlap Zones in Albinism

To further investigate whether the overlapping right and left hemifield representations in albinism are responsible for aberrant dual pRFs, we examined the association of overlap zones with the distribution of voxels having dual pRFs. Note that the overlap zones were computed from the hemifield ring stimuli while the dual pRFs were computed independently from the rotating wedge data. **Fig 4A** shows cortical surface models of subject 5's overlap map (left) with the corresponding clustered single-dual pRF map (right). Note that the large red patch of dual pRF voxels in V1 is closely associated with a green patch of hemifield overlap. However in V2 and V3, the majority of hemifield overlap bands failed to meet the dual pRF criteria in this subject.

To quantify the correspondence between the dual pRF clusters and HF overlap zones, in **Fig 4B** we calculated the proportion of dual pRF voxels which fell in non-overlap versus overlap zones. To be included in this analysis, voxels must have met the inclusion criteria for both the overlap and the pRF analysis described in Methods. For the subject displayed in **Fig 4A** (subject 5) the majority (~70%) of dual pRF voxels fell in the overlap zones. However, this relationship only held strongly for three of the five subjects with albinism: in subjects 1, 3, and 5 the majority (62-74%) of dual pRF voxels fell in R-L hemifield overlap zones. This relationship was less strong in subject 2 (54% of duals in overlap zones), and is reversed in subject 4. This latter seemingly illogical result led to the following analysis of the visual field locations of dual pRF components.

Dual pRF Symmetry

The discovery of voxels meeting our dual pRF criteria which were outside of hemifield overlap zones led us to question whether dual pRF voxels in our albinism subjects were necessarily responding to bilateral regions mirrored across the vertical meridian as suggested by previous work in achiasma (Hoffmann et al., 2012). To investigate this, we assessed the symmetry of dual pRFs by computing the angle formed by the two pRF centers with respect to horizontal. Example results from this analysis are displayed in **Fig 5** for two different subjects with albinism whose data are shown in separate columns. **Fig 5A** displays empirical rotating wedge timecourses (green) plus the predicted waveform (black) based on the dual pRF model shown in **Fig 5B**. Note that both timecourses contain ten robust, BOLD peaks even though the rotating wedge stimulus had only five cycles. In **Fig 5B** thin colored lines intersect the pRF centers to help visualize their respective angles. For subject 5 (left), the two pRF locations are nearly symmetrical across the vertical meridian as indicated by their near zero angle. However, this is clearly not the case for subject 3 (right). For subject 3, the two pRFs are in opposite hemifields, but instead fall at an angle of nearly 45 degrees with one pRF centered on the left horizontal meridian and the other situated near the lower vertical meridian.

To assess the overall patterns of dual pRF symmetry, **Fig 5C** plotshistograms of dual pRF angles for the two subjects. Subject 5's narrow distribution centered on 0 degrees indicates that, like the example above, the vast majority of dual pRFs were symmetrical across the vertical meridian. However, subject 3's distribution is shifted substantially leftward to be centered near -45 degrees, indicating that the majority of dual pRFs responded to angular positions offset by ~45 degrees from symmetrical as in the individual example in **Fig 5B.**

Fig 5D presents inflated surface models of the occipital showing the distribution of dual pRF angle across each subject's cortical surface. The color codes depicting dual pRF angle are shown above each image. Consistent with the histogram in **Fig 5C**, subject 5's dual pRF

clusters are mostly green (angle of ~0 degrees) indicating symmetry across the vertical meridian. The dual pRFs are heavily clustered in V1 but are also found in V2 and V3 albeit in lesser numbers. Subject 3 also has large clusters of dual pRF voxels in V1, V2, and V3 but they are mostly colored yellow-orange, indicating dual-pRF angles near 45 degrees.

Finally, to assess the visual field distributions of dual pRFs for subjects 3 and 5, we plotted pRF schematic profiles **(Fig 6)** for 25 voxels from each subject onto a map of the central 20 degrees of the visual field (**Fig 6**). These voxels represented those dual pRFs having the highest ΔVE explained by the dual model relative to the single model. In this figure, the blue circles represent the full width at half max for each dual pRF component with thin blue lines connecting the centers of each dual pRF pair. As illustrated for the single voxel in **Fig 5**, subject 5's dual pRFs (**Fig 6** left) all responded to roughly mirror symmetric locations across the vertical meridian but slightly below the horizontal meridian. This is roughly in accord with the anatomical location of the patch of highest ΔVE displayed in **Fig 2B** (yellow) that lies in dorsal V1 which would be consistent with a lower visual field representation. However, subject 3's dual pRFs (**Fig 6** right) are all ~45 degrees from horizontal symmetry with one component near the left horizontal meridian and one component near the lower vertical meridian. Together, the results of **Fig 5** and **Fig 6** indicate that the cortical distribution and configuration of dual pRFs can vary considerably across subjects with albinism and are not always mirror symmetric across the vertical meridian.

Discussion

In this study, we examined the functional organization of visual cortex in albinism subjects with a particular focus on aberrant retinotopy and the characteristics of single voxel, population receptive fields (pRFs). In all our subjects with albinism, we observed aberrant representations of the ipsilateral visual hemifield that were superimposed on the normal contralateral hemifield

representation within each occipital hemisphere, consistent with previous reports (Morland et al., 2001; Hoffmann et al., 2003; von dem Hagen et al., 2007; Kaule et al., 2014). It's worth noting that the phenotypes in our subjects included OA, OCA1B, and OCA2, indicating that such aberrant representations are not unique to any one albinism subtype. We predicted that such overlaid representations would result in single voxels having "dual" pRFs. Such voxels were numerous in three of our five subjects with albinism (subjects 2, 3, and 5) and were observed in the other two but in smaller, more diffusely distributed clusters often with noisier fMRI signals. Signal quality likely contributed to the smaller numbers of dual pRF voxels observed in subject 1; however, despite excellent overall signal quality in subject 4, we could find very few dual pRF voxels. It is notable that subject 4 is also the subject with the lowest percent hemifield overlap (**Fig 1C**).

Significantly, the symmetry of dual pRFs in subjects 2, 3 and 5 varied substantially by subject with subjects 2 and 5's dual pRFs being mostly mirror-symmetrical across the vertical meridian, and subject 3's dual pRFs being systematically asymmetrical. Together, these results indicate that retinocortical miswiring in albinism is more complex and varied than previously appreciated, thus indicating a need for extension and/or revision of current models of retinocortical miswiring in albinism.

Aberrant Retinotopic Organization in Albinism

We observed substantially overlapping right and left hemifield representations in each cortical hemisphere of all subjects with albinism. These zones of hemifield overlap were roughly centered on the vertical meridian representations at the borders of V1/V2 and the lateral border of V3 in each subject. This pattern is consistent with the retinal line of decussation, which is normally centered on the vertical meridian, having shifted temporally with the misrouted temporal afferents reaching the same locations in ipsilateral visual cortex as their

mirrored nasal counterparts. The mean percentage of cortex responding to both right and left hemifield stimuli varied significantly across subjects (30-50%), consistent with the known variability in extent of miswiring at the optic chiasm across the albinism population as a whole (Creel et al., 1981; Hoffmann et al., 2003; Hoffmann et al., 2005; von dem Hagen et al., 2007; Kaule et al., 2014). The observation that the percent overlap was relatively constant across V1-V3 within individuals (See **Fig 1**) suggests that the aberrant ipsilateral representation set up by the retinocortical afferents to V1 is propagated to subsequent stages of the visual hierarchy as suggested by (Wolynski et al., 2010; Kaule et al., 2014).

Subjects with Albinism Have Both Voxels with Single and Dual pRFs

Our pRF modeling analysis suggests that the partial superposition of opposite hemifield representations in albinism produces a complex mixture of voxels having either single or dual pRFs. This was qualitatively evident in the rotating wedge timecourse data as some voxels responded with ten robust peaks while others responded with only five, which was expected since our wedge stimulus completed only five rotations about the fixation point. For such voxels with ten peak responses, the dual pRF model typically explained significantly more variance than the single pRF model. In albinism subjects an average of 10% of visually responsive voxels in V1 met our dual pRF criteria with lower percentages observed in V2 and V3. By contrast, dual pRFs in control subjects were virtually absent which strongly indicates that those observed in subjects with albinism were not the result of some methodological artifact or simply the product of "partial voluming" across sulci.

Distribution of Dual pRF Voxels Relative to Hemifield Overlap Zones

Given the aberrant superposition of opposite hemifield representations within visual cortex of albinism subjects, one might expect that all voxels within these overlap zones would have dual

pRFs whereas voxels outside these zones would all have single pRFs. This was not the case. For three of our five subjects with albinism, dual pRF voxels did occur preferentially in regions of right-left hemifield overlap (**Fig4)**. The spatial patterns of dual pRF clusters in these subjects often closely matched those of the overlap zones, consistent with the notion that aberrant pRFs are a consequence of hemifield overlap. However, single pRF voxels were also numerous within overlap zones in all subjects with albinism, indicating that the occurrence of dual pRFs is not obligatory within hemifield overlap regions. However, it is important to note that the successful modeling of dual pRFs could only occur when the two peaks of each dual response (five dual peak pairs) were sufficiently separated to be fit better by the dual pRF model compared to a "wide" single pRF model. This was often not true for dual pRFs close to the vertical meridian. As a result, our measure of dual pRF prevalence is likely to be an under-estimate, which would also reduce the correlation between hemifield overlap zones and dual pRFs.

Asymmetric Dual pRFs in Albinism

Based on reports of dual pRFs in achiasma (Hoffmann et al., 2012), we did not expect to find numerous voxels with asymmetric dual pRFs (**Fig 5A-B**). Indeed for some subjects, the majority of dual pRFs were symmetric across the midline (though with a variety of separations) consistent with the model of retinocortical miswiring posited by Hoffmann (Hoffmann et al., 2003). However, in one subject (subject 5), many dual pRFs occurred in clusters having asymmetrical components, all with roughly the same orientation. These asymmetric dual pRFs are not predicted by current models of misrouting and suggest wiring anomalies that are more complicated than a symmetrical right-left decussation error.

What do Dual pRF Asymmetries Tell us About Retinocortical Miswiring in Albinism?

The asymmetric dual pRFs modeled in this study suggest that in addition to misrouting of the temporal retinal afferents to the improper cortical hemisphere there is also miswiring of afferents to improper retinotopic locations within a given hemisphere, at least in some subjects with albinism.

Consider the dual pRF topography of subject 3 (**Fig 5B)**. This voxel was located in the fundus of the calcarine sulcus of the left hemisphere, which would normally be the locus of the right horizontal meridian. The dual pRF component of this voxel that sits on the left horizontal meridian is therefore aberrantly represented in the wrong (ipsilateral) hemisphere. However, the pRF component in the right visual field is close to the inferior vertical meridian, so it is represented in the proper hemisphere but at an aberrant location close to the vertical rather than horizontal meridian. In this way, neither pRF component is "normal," and there is a superposition of incongruent meridian representations as well as opposite hemifield representations. This pRF topography cannot be explained by a simple decussation error at the optic chiasm, but instead implicates more complicated and heterogenous patterns of retinocortical miswiring both within and between hemispheres.

Alternative Explanations for Dual pRFs and Asymmetry

The discovery of dual pRFs in albinism was anticipated given the previously known superposition of opposite hemifield representations in visual cortex. Nevertheless, artefactual causes might include "partial voluming" of retinotopically disparate locations across sulci or across the midline. Although we can not entirely rule out the possibility that some optimally situated voxels might show such effects, dual pRF voxels often occur in large clusters with many voxels situated entirely within gray matter. Moreover, if such effects were common, then

we would expect to observe comparable numbers of dual pRFs in our control subjects for whom the incidence was virtually zero.

Another concern is that our asymmetric dual pRFs might arise from improper calibration of the raw temporal phase delay values that encode the polar angle coordinate of pRF location. One factor that could affect this is the sluggishness of the BOLD hemodynamic response which if not correctly estimated could cause a dual pRF to be "rotated" relative to its true position in the visual field. To rule this out, we tested the potential effect of hemodynamic response functions having different temporal delays on our dual pRF fits. We could find no physiologically plausible HRF delay that could force our asymmetric dual pRFs to become mirror symmetric.

pRF Modeling in Albinism May Provide the Key to Uncovering Hidden Perceptual Deficits

Perhaps the most intriguing aspect of marked retinotopic disorganization in albinism is that it has not been shown to produce any major perceptual or behavioral deficit except perhaps a loss of stereopsis which would logically follow upon the loss of ocular dominance columns which are reported to be supplanted by "hemifield columns" (Guillery et al., 1984; Olman et al., 2018). Initially, the highly aberrant superposition of opposite hemifield representations in V1-V3 would lead one to expect some form of perceptual interaction or competition between widely disparate locations in the two visual hemifields. Indeed, the discovery of dual pRF voxels might provide a specific neural basis for such interactions. However, the highly irregular spatial arrangement of dual pRFs that we show here suggests that previous attempts to demonstrate perceptual interactions between the right and left hemifields (Hoffmann et al., 2007; Klemen et al., 2012) may have failed to test the appropriate locations in the visual field that are associated with the idiosyncratic pattern of dual pRFs in each albinism subject. Thus, to expose potentially hidden perceptual interactions it would be advisable to first perform a

detailed study of dual pRFs in each subject and create a visual field map (**Fig 6**) of locations that might potentially interact.

Implications for Developmental Understanding of Retinotopy

Finally, it has long been known that the albinism population is genetically heterogenous (Montoliu et al., 2014; Patel et al., 2019). Different genetic mutations in the melanin synthesis pathway give rise to different subtypes of albinism as well as heterogeneity in retinal morphology (Oetting and King, 1999; Simeonov et al., 2013; Wilk et al., 2014b; Prieur and Rebsam, 2017; Kruijt et al., 2018; Lee et al., 2018). However, specific genetic details for individual patients have not been included in the vast majority of previous imaging studies of albinism. In this study, we intentionally selected albinism subjects to represent a diverse sampling of albinism subtypes (**Table 1**) in order to enhance the probability of observing variation in the central organization of visual pathways. Interestingly we saw disrupted central organization even in subjects with the newly discovered “tri-allelic” form of albinism (Norman et al., 2017; Monferme et al., 2018; Gronskov et al., 2019). Though our sample is not nearly large enough to draw strong correlations between genetic, retinal and central factors, we did observe significant variation across our albinism sample in the extent of hemifield overlap and in the incidence and symmetry of dual pRFs. We speculate that genetic factors responsible for the range of subtypes in albinism may also underlie the variations in retinocortical organization observed in our dual pRF analysis. If so, this suggests that in a larger sample of subjects with albinism, this approach will prove increasingly productive for linking peripheral genetic and morphological factors with associated central mechanisms and their ultimate behavioral consequences not only in albinism but in a variety of inherited vision disorders (Hoffmann and Dumoulin, 2015).

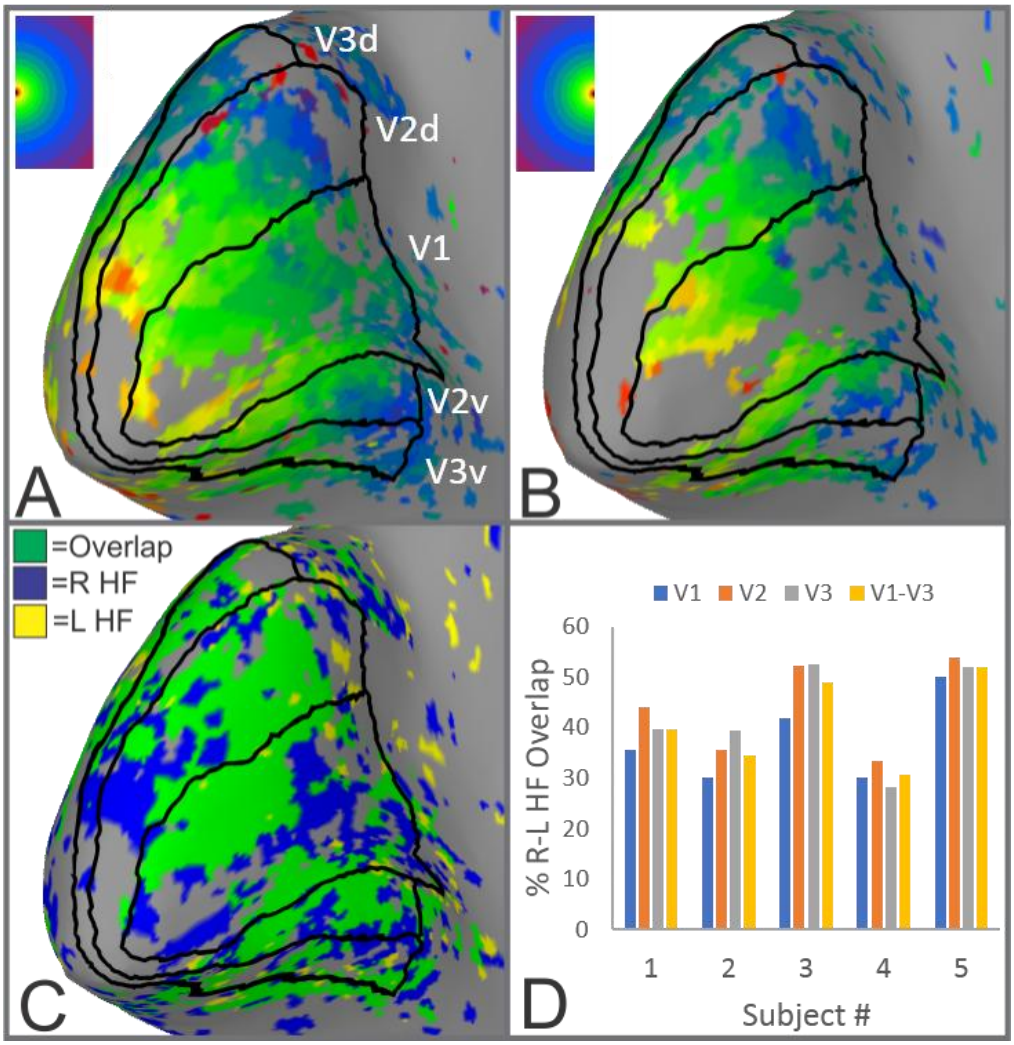

Figure 1: Monocular (right eye) hemifield eccentricity maps and overlap. (A) Right hemifield stimulus condition. (B) Left hemifield stimulus condition. (C) Hemifield overlap map. Green is logical intersection of A and B after thresholding. (D) Percent hemifield overlap in V1-V3. Data combined across all eye-hemifield stimulus conditions. Color codes for eccentricity and overlap maps are in upper left corner of A-C. Thin black lines demarcate V1-V3 visual area boundaries. All maps are displayed on left occipital cortex surface model for a representative subject with albinism.

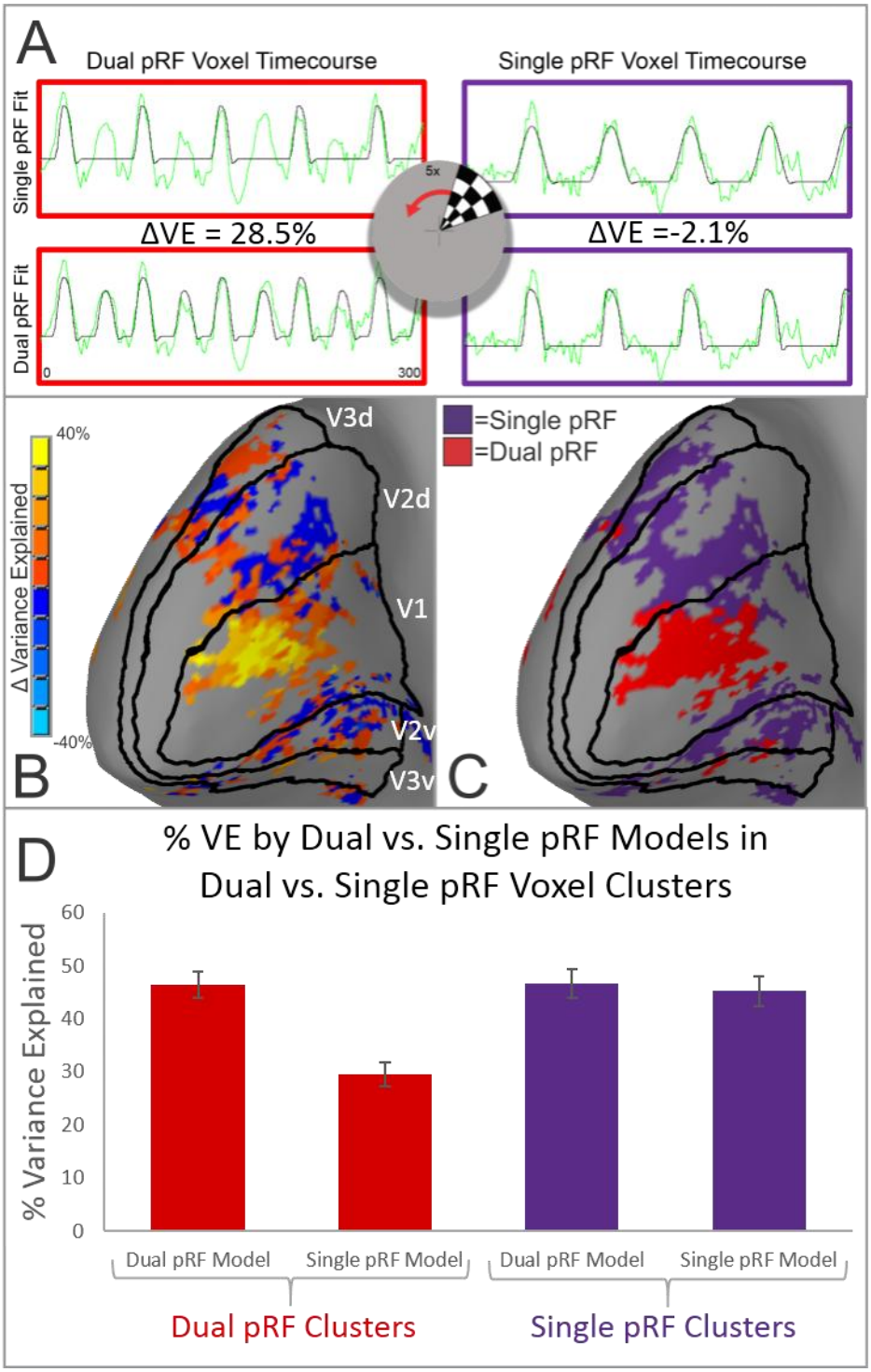

Figure 2: Timecourse and distribution of single vs dual pRF voxels for one subject with albinism. (A) Representative fMRI timecourse (green) for voxel classified as dual pRF (red outline, left) and single pRF (purple outline, right). Single (top) vs dual (bottom) pRF model predictions shown in black. Overlay depicts single frame of rotating wedge stimulus. (B) Brain map of % difference in fMRI signal variance explained by dual vs single pRF models (ΔVE =

$\%VE_{dual}$ - $\%VE_{single}$). Color code at left. (C) Distribution of single (purple) vs dual (red) pRF voxels as determined by our clustering analysis. (D) Mean % fMRI signal variance explained by single vs dual pRF models for clusters of ten or more dual pRF voxels (red, left) versus clusters of single pRF voxels (purple, right). Mean values are for all five subjects with albinism. Error bars indicate standard error of the mean. The dual pRF model explains significantly more variance (17% more) in dual pRF clusters than in single pRF clusters. (paired two tailed t-test, $p < .001$) The dual pRF model also explained significantly more variance in the single pRF clusters; however, the magnitude of the difference was very small (1%).

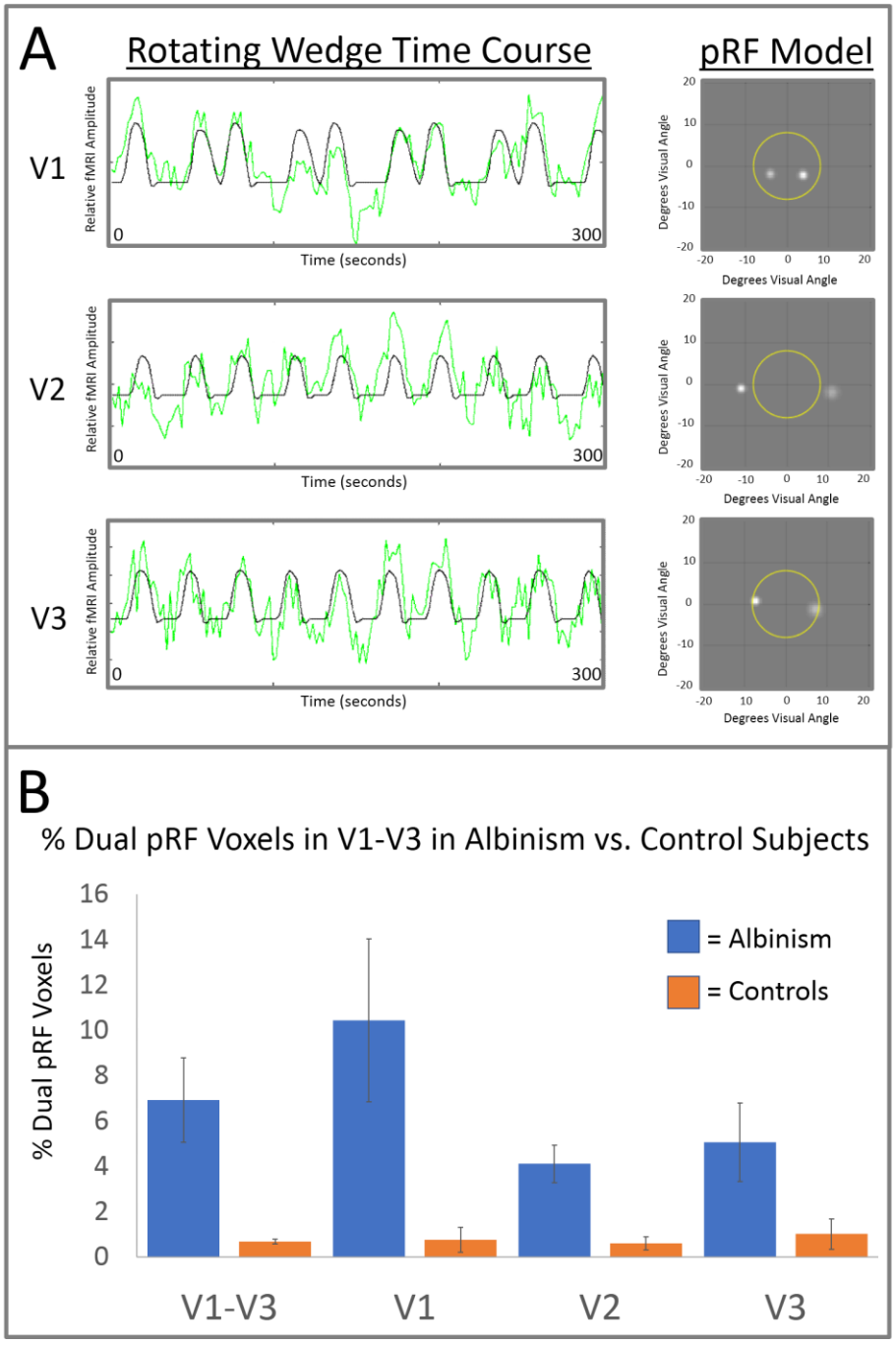

Figure 3: (A) fMRI timecourses (green) and pRF model predictions (black) for representative voxels in V1-V3 of one subject with albinism. Right: Dual pRF models in visual space. White spots represent gaussian amplitude profiles for each dual pRF component. Yellow ring marks 8 degrees eccentricity. (B) Percent dual pRF voxels in V1-V3 in subjects with albinism (blue) and controls (orange) which met our %ΔVE and clustering criteria (see text for details).

Subjects with albinism had significant numbers of dual pRF voxels whereas control subjects had virtually none.

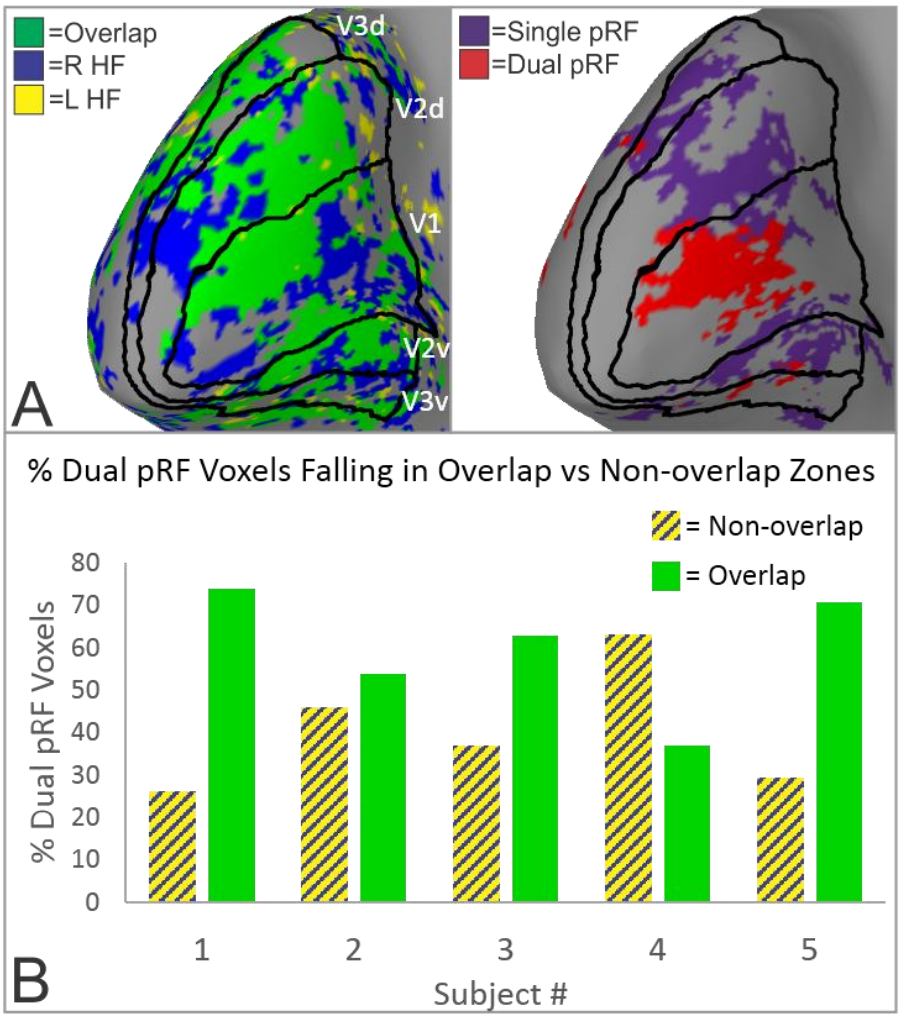

Figure 4: Dual pRF voxels often coincide with right-left hemifield overlap zones. (A) Repeat of Figures 1C and 2C. Note close correspondence of red dual-pRF cluster (right) with large green overlap zone (left). (B) Percent of dual pRF voxels in overlap vs non-overlap zones for all 5 subjects with albinism.

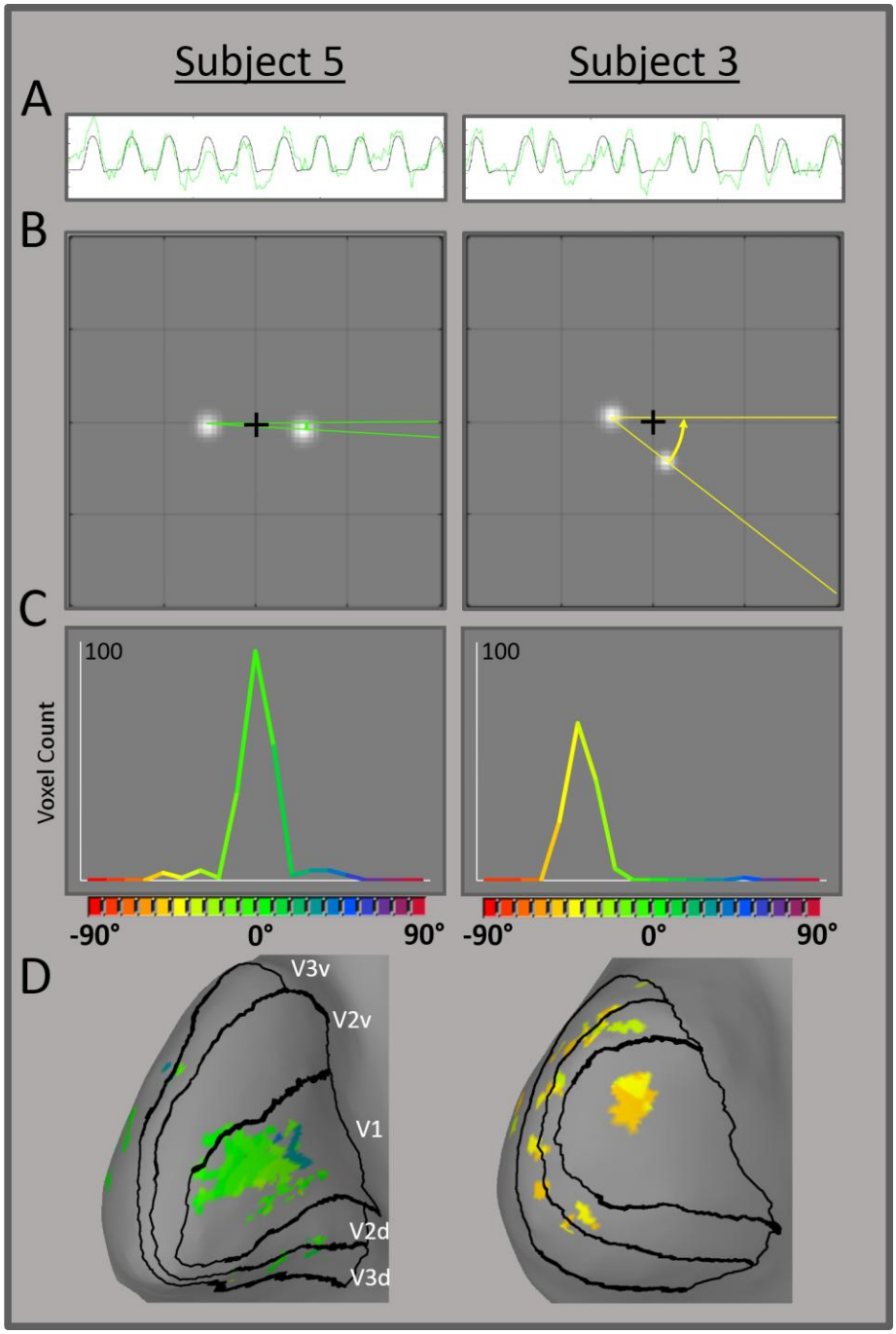

Figure 5: Dual pRF symmetry varies across subjects with albinism. (A) fMRI responses (green) and dual pRF model predictions (black) for representative voxels whose dual pRF profiles (B) illustrate either mirror symmetric (left) or tilted (right) configurations. (C) Histograms of dual pRF angles relative to horizontal meridian for different subjects with albinism (3 and 5). (D) Left occipital cortex surface maps for same subjects showing dual pRF clusters having similar within-cluster pRF angles but different angles across subjects (green vs yellow). A 45°

difference in mean pRF angle corresponds to a 15 sec difference in temporal phase of the fMRI signal, too large to be explained by BOLD hemodynamic variation.

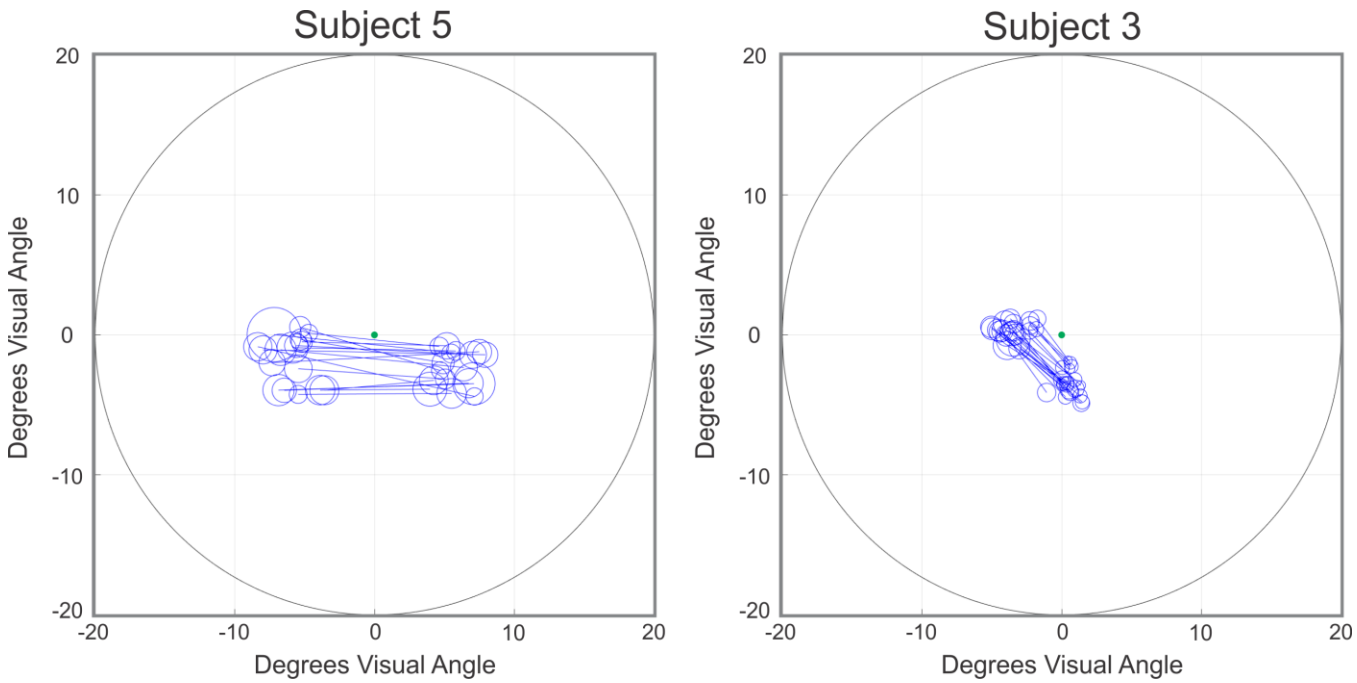

Figure 6: Visual field plots of 25 dual pRFs with largest ΔVE's for the two subjects with albinism (3 and 5) whose dual pRF histograms are illustrated in Fig. 5. Blue circles represent full width at half maximum of each dual pRF component. Centers of each dual pRF pair are connected by a thin line. Subject 5's dual pRFs are all approximately mirror symmetric. Subject 3's dual pRFs are tilted nearly 45° and centered on orthogonal meridia, both components being aberrant (see text for details).

REFERENCES

Ahmadi K, Fracasso A, van Dijk JA, Kruijt C, van Genderen M, Dumoulin SO, Hoffmann MB (2018) Altered organization of the visual cortex in FHONDA syndrome. Neuroimage.

Amano K, Wandell BA, Dumoulin SO (2009) Visual field maps, population receptive field sizes, and visual field coverage in the human MT+ complex. J Neurophysiol 102:2704-2718.

Arcaro MJ, McMains SA, Singer BD, Kastner S (2009) Retinotopic organization of human ventral visual cortex. J Neurosci 29:10638-10652.

Bandettini PA, Jesmanowicz A, Wong EC, Hyde JS (1993) Processing strategies for time-course data sets in functional MRI of the human brain. Magnetic Resonance in Medicine 30:161-173.

Cox RW (1996) AFNI: Software for analysis and visualization of functional magnetic resonance neuroimages. Computers and Biomedical Research 29:162-173.

Creel D, Spekreijse H, Reits D (1981) Evoked potentials in albinos: efficacy of pattern stimuli in detecting misrouted optic fibers. Electroencephalogr Clin Neurophysiol 52:595-603.

Datta R, DeYoe EA (2009) I know where you are secretly attending! The topography of human visual attention revealed with fMRI. Vision Res 49:1037-1044.

DeYoe EA, Carman G, Bandettini P, Glickman S, Wieser J, Cox R, Miller D, Neitz J (1996) Mapping striate and extrastriate visual areas in human cerebral cortex. Proc Natl Acad Sci USA 93:2382-2386.

Dumoulin SO, Wandell BA (2008) Population receptive field estimates in human visual cortex. Neuroimage 39:647-660.

Engel SA, Glover GH, Wandell BA (1997) Retinotopic organization in human visual cortex and the spatial precision of functional MRI. Cereb Cortex 7:181-192.

Gronskov K, Jespersgaard C, Bruun GH, Harris P, Brondum-Nielsen K, Andresen BS, Rosenberg T (2019) A pathogenic haplotype, common in Europeans, causes autosomal recessive albinism and uncovers missing heritability in OCA1. Sci Rep 9:018-37272.

Guillery RW, Hickey TL, Kaas JH, Felleman DJ, Debruyn EJ, Sparks DL (1984) Abnormal central visual pathways in the brain of an albino green monkey (Cercopithecus aethiops). J Comp Neurol 226:165-183.

Hansen KA, Kay KN, Gallant JL (2007) Topographic organization in and near human visual area V4. J Neurosci 27:11896-11911.

Hoffmann MB, Dumoulin SO (2015) Congenital visual pathway abnormalities: a window onto cortical stability and plasticity. Trends Neurosci 38:55-65.

Hoffmann MB, Seufert PS, Schmidtborn LC (2007) Perceptual relevance of abnormal visual field representations: static visual field perimetry in human albinism. Br J Ophthalmol 91:509-513.

Hoffmann MB, Tolhurst DJ, Moore AT, Morland AB (2003) Organization of the visual cortex in human albinism. J Neurosci 23:8921-8930.

Hoffmann MB, Lorenz B, Morland AB, Schmidtborn LC (2005) Misrouting of the optic nerves in albinism: estimation of the extent with visual evoked potentials. Invest Ophthalmol Vis Sci 46:3892-3898.

Hoffmann MB, Kaule FR, Levin N, Masuda Y, Kumar A, Gottlob I, Horiguchi H, Dougherty RF, Stadler J, Wolynski B, Speck O, Kanowski M, Liao YJ, Wandell BA, Dumoulin SO (2012) Plasticity and stability of the visual system in human achiasma. Neuron 75:393-401.

Horton JC, Hoyt WF (1991) The representation of the visual field in human striate cortex. A revision of the classic holmes map. Arch Ophthalmol 109:816-824.

Kaule FR, Wolynski B, Gottlob I, Stadler J, Speck O, Kanowski M, Meltendorf S, Behrens-Baumann W, Hoffmann MB (2014) Impact of chiasma opticum malformations on the organization of the human ventral visual cortex. Hum Brain Mapp 35:5093-5105.

Klemen J, Hoffmann MB, Chambers CD (2012) Cortical plasticity in the face of congenitally altered input into V1. Cortex; a journal devoted to the study of the nervous system and behavior 48:1362-1365.

Kruijt CC, de Wit GC, Bergen AA, Florijn RJ, Schalij-Delfos NE, van Genderen MM (2018) The Phenotypic Spectrum of Albinism. Ophthalmology 125:1953-1960.

Lee DJ, Woertz EN, Visotcky A, Wilk MA, Heitkotter H, Linderman RE, Tarima S, Summers CG, Brooks BP, Brilliant MH, Antony BJ, Lujan BJ, Carroll J (2018) The Henle Fiber Layer in Albinism: Comparison to Normal and Relationship to Outer Nuclear Layer Thickness and Foveal Cone Density. Invest Ophthalmol Vis Sci 59:5336-5348.

Monferme S, Lasseaux E, Duncombe-Poulet C, Hamel C, Defoort-Dhellemmes S, Drumare I, Zanlonghi X, Dollfus H, Perdomo Y, Bonneau D, Korobelnik JF, Plaisant C, Michaud V, Pennamen P, Rooryck-Thambo C, Morice-Picard F, Paya C, Arveiler B (2018) Mild form of oculocutaneous albinism type 1: phenotypic analysis of compound heterozygous patients with the R402Q variant of the TYR gene. Br J Ophthalmol 24:2018-312729.

Montoliu L, Gronskov K, Wei AH, Martinez-Garcia M, Fernandez A, Arveiler B, Morice-Picard F, Riazuddin S, Suzuki T, Ahmed ZM, Rosenberg T, Li W (2014) Increasing the complexity: new genes and new types of albinism. Pigment Cell Melanoma Res 27:11-18.

Morland AB, Baseler HA, Hoffmann MB, Sharpe LT, Wandell BA (2001) Abnormal retinotopic representations in human visual cortex revealed by fMRI. Acta psychologica 107:229-247.

Norman CS, O'Gorman L, Gibson J, Pengelly RJ, Baralle D, Ratnayaka JA, Griffiths H, Rose-Zerilli M, Ranger M, Bunyan D, Lee H, Page R, Newall T, Shawkat F, Mattocks C, Ward D, Ennis S, Self JE (2017) Identification of a functionally significant tri-allelic genotype in the Tyrosinase gene (TYR) causing hypomorphic oculocutaneous albinism (OCA1B). Sci Rep 7:017-04401.

Oetting WS, King RA (1999) Molecular basis of albinism: mutations and polymorphisms of pigmentation genes associated with albinism. Human mutation 13:99-115.

Oetting WS, Summers CG, King RA (1994) Albinism and the associated ocular defects. Metabolic, pediatric, and systemic ophthalmology 17:5-9.

Olman CA, Bao P, Engel SA, Grant AN, Purington C, Qiu C, Schallmo MP, Tjan BS (2018) Hemifield columns co-opt ocular dominance column structure in human achiasma. Neuroimage 164:59-66.

Patel A et al. (2019) The Oculome Panel Test: Next-Generation Sequencing to Diagnose a Diverse Range of Genetic Developmental Eye Disorders. Ophthalmology 14:050.

Pitzalis S, Sereno MI, Committeri G, Fattori P, Galati G, Patria F, Galletti C (2010) Human v6: the medial motion area. Cereb Cortex 20:411-424.

Pitzalis S, Galletti C, Huang RS, Patria F, Committeri G, Galati G, Fattori P, Sereno MI (2006) Wide-field retinotopy defines human cortical visual area v6. J Neurosci 26:7962-7973.

Prieur DS, Rebsam A (2017) Retinal axon guidance at the midline: Chiasmatic misrouting and consequences. Dev Neurobiol 77:844-860.

Puckett AM, DeYoe EA (2015) The attentional field revealed by single-voxel modeling of FMRI time courses. J Neurosci 35:5030-5042.

Saad ZS, DeYoe EA, Ropella KM (2003) Estimation of FMRI response delays. Neuroimage 18:494-504.

Sereno MI, Pitzalis S, Martinez A (2001) Mapping of contralateral space in retinotopic coordinates by a parietal cortical area in humans. Science 294:1350-1354.

Sereno MI, Dale AM, Reppas JB, Kwong KK, Belliveau JW, Brady TJ, Rosen BR, Tootell RBH (1995) Borders of multiple visual areas in humans revealed by functional MRI. Science 268:889-893.

Silver MA, Kastner S (2009) Topographic maps in human frontal and parietal cortex. Trends Cogn Sci 13:488-495.

Simeonov DR, Wang X, Wang C, Sergeev Y, Dolinska M, Bower M, Fischer R, Winer D, Dubrovsky G, Balog JZ, Huizing M, Hart R, Zein WM, Gahl WA, Brooks BP, Adams DR (2013) DNA variations in oculocutaneous albinism: an updated mutation list and current outstanding issues in molecular diagnostics. Human mutation 34:827-835.

Swisher JD, Halko MA, Merabet LB, McMains SA, Somers DC (2007) Visual topography of human intraparietal sulcus. J Neurosci 27:5326-5337.

von dem Hagen EA, Houston GC, Hoffmann MB, Morland AB (2007) Pigmentation predicts the shift in the line of decussation in humans with albinism. The European journal of neuroscience 25:503-511.

Wandell BA, Winawer J (2011) Imaging retinotopic maps in the human brain. Vision Research 51:718-737.

Wandell BA, Dumoulin SO, Brewer AA (2007) Visual field maps in human cortex. Neuron 56:366-383.

Wilk MA, Mathis J, Summers CG, Carroll J, DeYoe E (2014a) Retino-cortical relationships in albinism. Journal of Vision 14:51.

Wilk MA, Wilk BM, Langlo CS, Cooper RF, Carroll J (2017) Evaluating outer segment length as a surrogate measure of peak foveal cone density. Vision Res 130:57-66.

Wilk MA, McAllister JT, Cooper RF, Dubis AM, Patitucci TN, Summerfelt P, Anderson JL, Stepien KE, Costakos DM, Connor TB, Jr., Wirostko WJ, Chiang PW, Dubra A, Curcio CA, Brilliant MH, Summers CG, Carroll J (2014b) Relationship between foveal cone specialization and pit morphology in albinism. Invest Ophthalmol Vis Sci 55:4186-4198.

Woertz EN, Wilk MA, Duwell E, Mathis J, Carroll J, DeYoe EA (2019) Retinal and Cortical Determinants of Cortical Magnification in Human Albinism. bioRxiv:562249.

Wolynski B, Kanowski M, Meltendorf S, Behrens-Baumann W, Hoffmann MB (2010) Self-organisation in the human visual system--visuo-motor processing with congenitally abnormal V1 input. Neuropsychologia 48:3834-3845.